Improvement of plasmonic field-matter interaction by subwavelength dielectric gratings

Nak-Hyeon Kim · Kyung Min Byun · Seung Ho Choi · Young L. Kim

Abstract We experimentally and theoretically investigate that detection sensitivity in surface plasmon resonance (SPR) biosensors can be significantly enhanced by employing subwavelength dielectric gratings deposited on a gold film. The enhancement originates from an improvement of field-matter interaction: enhanced evanescent field intensity at the binding region and increased surface reaction area. Using a large-area SiO_2 grating array fabricated by nanoimprint lithography, experimental sensor performance measured by parylene film coating shows that the SPR substrates combined with a dielectric grating provide a notable sensitivity improvement compared to a conventional bare gold film. We also demonstrate that plasmon field can be more confined and enhanced at the dielectric gratings with a larger width. The proposed SPR structure could potentially be useful in a variety of plasmonic applications including high-sensitivity biosensors.

1 Introduction

Despite several unique advantages such as rapid, quantitative, and label-free detection, conventional surface plasmon resonance (SPR) biosensors often suffer from insufficient sensitivity, especially for biomolecules at very low molecular weights [1]. Among numerous approaches which have emerged to address this issue [2–5], guided-wave SPR configuration with an insertion of a thin dielectric film between the metal layer and the analyte region has gained much attention in recent years. For example, Lahav et al. proved its effectiveness in enhancing the sensor sensitivity by introducing a thin silicon layer on top of a silver film [6]. The enhancement was primarily due to an increase in the interaction volume (i.e., the evanescence depth) and an increase in the plasmon field intensity at the analyte region [7]. The improved penetration depth can be useful to investigate a bulk change in the refractive index for gas sensing or cell analysis applications [8].

On the other hand, when layered biointeractions occur at the sensor substrate in nanoscale distance, the deep penetration of surface plasmons into the sensing medium is not advantageous. In this case, an alternative approach is to realize a significant extension of surface-limited reaction area, which can be advantageous for an enhanced detection of molecular binding events. For example, we have recently reported a notable sensitivity improvement by incorporating rough surface of an indium tin oxide (ITO) layer on a gold film [9]. Porous ITO layers fabricated by e-beam evaporation and angled deposition can provide more binding spaces than an ideally flat surface. This further increases the number of ligands and target molecules that participate in the binding interaction, producing a higher resonance shift. However, while the use of porous dielectric film is a simple and effective method, its practical applicability is limited due to the fact that only the pores in the vicinity of the ITO surface are exposed to the biointeraction. In addition, inherent structural defects make the injected analytes inaccessible into the embedded pores.

In this respect, we have numerically investigated an alternative SPR scheme to improve the sensor performance by employing a subwavelength dielectric grating [10]. Compared with the previous study based on metallic

N.-H. Kim · K. M. Byun (✉)
Department of Biomedical Engineering, Kyung Hee University,
Yongin 446-701, Korea
e-mail: kmbyun@khu.ac.kr

S. H. Choi · Y. L. Kim
Weldon School of Biomedical Engineering, Purdue University,
West Lafayette, IN 47907, USA

nanogratings [11], the exploitation of well-defined dielectric nanoarrays can offer advantages of deep absorption band and performance reproducibility, while maintaining the profit of a high sensitivity. Rapid advances in the nanofabrication technology allow for manipulating the optical properties of nanoscale devices for specific applications in a controllable manner. In particular, the improved sensitivity performance can be attributable to enhanced field-matter interactions: (1) an increased surface adhesion area and (2) a strong interaction between the bound analytes and the enhanced plasmon field. In this paper, our experimental and numerical study reveals that the dielectric grating-based SPR scheme has the great potential for improving the sensor sensitivity, superior to the conventional SPR biosensors. Thus, our study will serve as the first step to demonstrate the feasibility of field-matter interaction improvement caused by dielectric gratings for sensitive SPR detection.

In the first part, we present experimental results of fabricating a large-area dielectric grating pattern via nanoimprint lithography (NIL). Second, to demonstrate a signal enhancement induced by subwavelength dielectric gratings, we measure the sensitivity characteristic by depositing a parylene film and compare the results with the case of a conventional SPR substrate. Third, we quantitatively analyze an effect of grating width on the sensor sensitivity, and this approach can give us a hint for achieving a higher sensitivity. Based on these results, we finally discuss underlying mechanisms of the electromagnetic field enhancement and propose an optimal configuration for a high-sensitivity biosensor application.

2 Experimental details

2.1 Sample Fabrication

Taking account of the advantages such as large-area grating pattern, robustness to fabrication error, and reliability in experiments, we utilized NIL in fabricating subwavelength dielectric gratings on a thin gold film. NIL is based on the direct mechanical deformation of the resist. The resolution achievable with NIL is beyond the limitations caused by light diffraction or beam scattering in other optical lithographies [12].

As shown in Fig. 1, a 45-nm-thick gold film was deposited onto an SF10 glass after an evaporation of a 2-nm-thick-chromium adhesion layer. A SiO_2 layer with a thickness of 100 nm was then grown on the gold film via a thermal oxidation method. Before pressing the stamp which contains a designed grating structure into the imprint resist (NIP-SC58LV100, Chem Optics, Korea), an additional coating of polymethyl methacrylate (PMMA) was
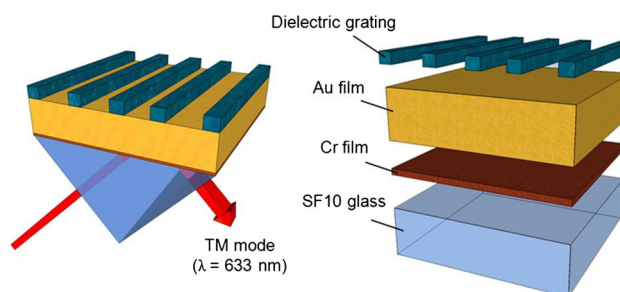

Fig. 1 Schematic of the proposed SPR system with a subwavelength dielectric grating. A thin gold film is deposited on a SF10 glass substrate via adhesion of a chromium layer. *Rectangular* dielectric gratings with a width w, a period Λ, and a thickness d are deposited on the gold/SF10 substrate. TM-polarized light with $\lambda = 633$ nm is incident with an angle of θ

applied so that the PMMA film acts as a cushioning layer that protects fragile nanosized features on the stamp surface. During the patterning process of transferring the imprinted patterns to dielectric gratings, a large-area stamp with high feature density created a deep thickness contrast of about 150 nm in the imprint resist. After the stamp was peeled off from the substrate, the PMMA and SiO_2 layers were removed by O_2 plasma etching for 120 s and anisotropic dry etching with a 9:1 SF_6-O_2 mixture for 60 s, respectively. Finally, the lift-off approach was used to remove the residual polymers. Figure 2 shows the cross-section and top view images of the fabricated samples based on SiO_2 gratings using scanning electron microscopy (SEM). Dielectric gratings have a rectangular profile with $\Lambda = 400$ nm, a width of $w = 200$ nm, and a thickness of $d = 100$ nm. The total size of dielectric grating pattern was approximately 5×5 mm^2.

2.2 Optical Measurement Setup

The fabricated samples were loaded into a custom-made SPR measurement setup to find the resonance angle in real time. Incident light from a He–Ne laser of $\lambda = 633$ nm was passed through a polarizer to produce a transverse magnetic (TM) mode signal. An optical chopper and a lock-in amplifier were employed to reduce an overall noise level. Reflected light from the sample was calibrated by a photodiode as an optical detector. Our SPR setup was based on dual concentric motorized rotation stages for angle scanning measurement with a nominal angular resolution of 0.002°. During the experiments, SPR curves were measured with a resolution of 0.01°.

2.3 Parylene film deposition

To test the sensor sensitivity improvement, a parylene film was applied on the substrate and the sensor sensitivity was
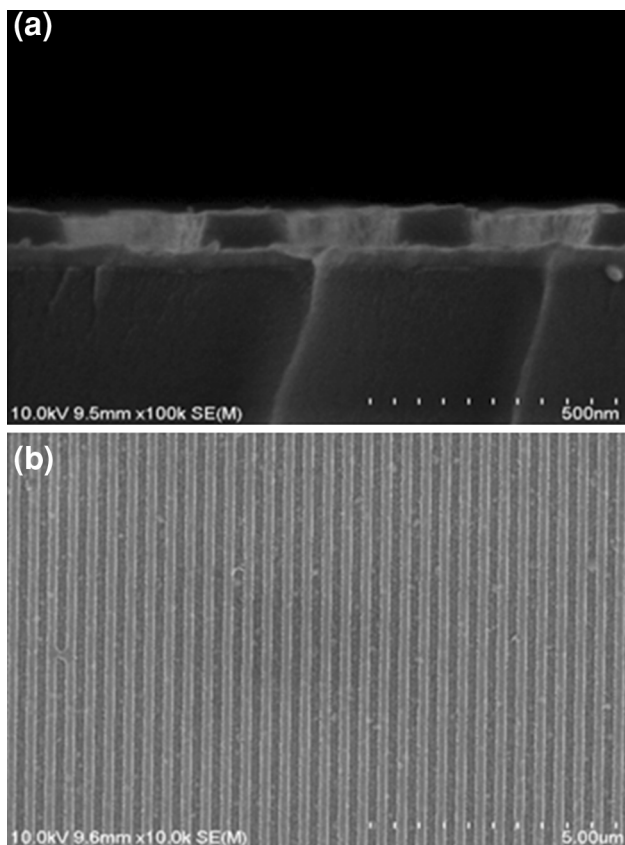
Fig. 2 **a** Cross-section and **b** top view SEM images of the fabricated array pattern of SiO$_2$ gratings on a gold/SF10 glass substrate

estimated by comparing the resonance angles before and after the film deposition. Although the sensitivity obtained from layered biointeractions such as DNA hybridization and protein–protein reaction could be a more practical performance measure, the degree of biomolecular interactions cannot be identical for gold and SiO$_2$ surfaces as the immobilization efficiency of the ligands varies with the substrate material. On the other hand, this method using a parylene film can reduce such experimental variances. Indeed, a parylene film has been frequently used as a linker layer to promote the covalent immobilization of proteins in SPR biosensing applications [13].

The deposition procedure of a parylene film was as follows: The fabricated SPR samples were first rinsed with distilled water for 5 min to remove any residues. After an evaporation of dimer at 160 °C and a pyrolysis process at 650 °C, a parylene layer was coated on the substrate at room temperature. The whole process was reproducibly carried out by a microprocessor-controlled parylene coater. The thickness of the parylene film was controlled by the initial amount of parylene dimer at a fixed deposition pressure. The deposition rate was 0.4 nm/mg for parylene-C averaged from four measurements.

2.4 Numerical methods

We used the rigorous coupled-wave analysis (RCWA) method to calculate light absorption characteristics of the dielectric grating-based SPR substrates. RCWA has been successfully applied to describe experimental results of periodic patterns [14, 15]. The light source was defined as a plane wave under TM polarization, and the illumination angle (θ) was scanned with a resolution of 0.01°. Details of RCWA can be found elsewhere [16–18]. For the simulation presented in this study, 30 spatial harmonics have been employed, unless otherwise noted. Finite-difference time-domain (FDTD) method was also used to visualize the near-field distribution. The minimum grid size for the FDTD was set to be 1 nm. The optical constants of SF10, chromium, and gold were obtained to be 1.723, $3.48 + 4.36i$, and $0.18 + 3.00i$ at $\lambda = 633$ nm from Ref. 18. The refractive index of the dielectric grating was assumed to be 1.457, which corresponds to the refractive index of SiO$_2$ [19].

3 Results and discussion

Figure 3 shows reflectance curves of conventional and SiO$_2$ grating-based SPR structures when a parylene layer forms a 5-nm-thick uniform coverage over the sensor substrates. The solid black and red lines indicate the curves before and after the deposition of parylene film in an air environment, respectively. For bare gold film without SiO$_2$ gratings, the resonance angle shifts from 38.87° to 39.01°; thus, the net change is 0.14°. However, the SPR substrate with a dielectric grating exhibits a larger shift of 0.32° in resonance angle, implying an improvement in sensitivity by 2.3 times.

Curve broadening in Fig. 3b should also be taken into consideration in evaluating the sensor performance, as it may affect the quality factor such as limit of detection (LOD), which was defined as the smallest change in the refractive index that produces a detectable change in the sensor output [20]. Based on the simple relation of LOD $= \sigma/S$, where σ is the standard deviation of noise of the sensor signal and S is the sensor sensitivity, the LOD gets worse due to an increased uncertainty caused by the broad and shallow SPR curves. By determining the signal quality parameters of curve width and minimum reflectance from Fig. 3, we find that the proposed SPR structure with a dielectric grating exhibits 1.7 times better LOD performance, compared to a conventional SPR system. Due to inevitable signal broadening caused by resonance excitation of surface plasmons in a higher momentum, the LOD improvement is not as high as the case of sensitivity.

More samples were also tested to verify the consistency of our experimental data. The mean values and standard
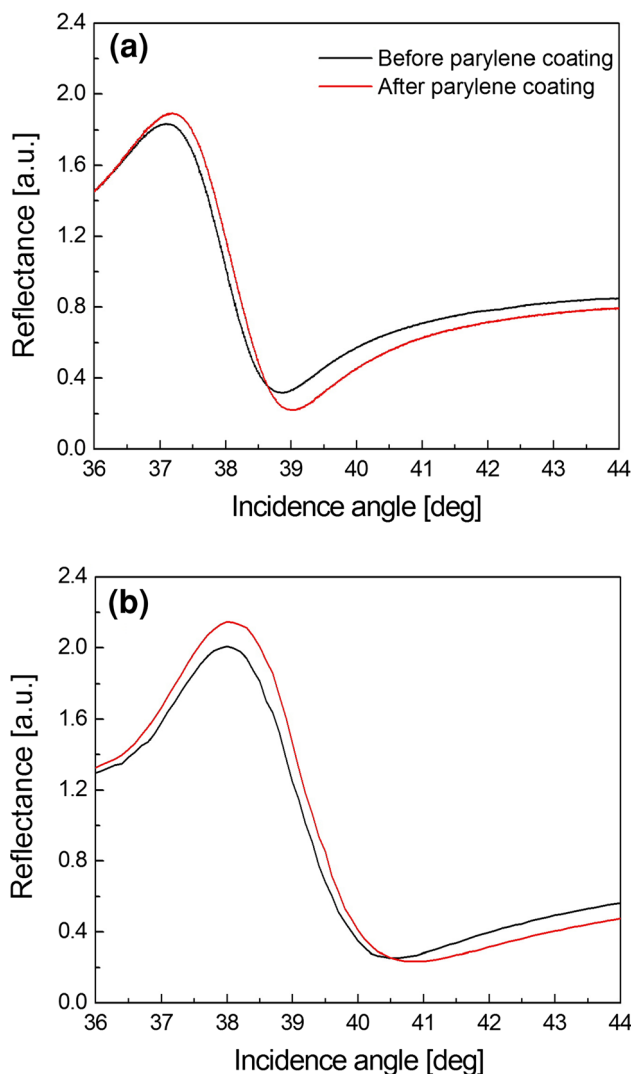
Fig. 3 SPR *curves* obtained from parylene coating experiments **a** for conventional bare gold substrate and **b** for SPR substrate with a SiO$_2$ grating of $\Lambda = 400$ nm, $w = 200$ nm, and $d = 100$ nm. The *black* and *red lines* represent the results before and after depositing a 5-nm-thick parylene film, respectively

errors in SPR angle shift were determined as $0.15° \pm 0.007°$ for conventional SPR substrates and $0.32° \pm 0.038°$ for SiO$_2$ grating-based ones, respectively. Thus, the sensitivity enhancement factor (SEF), defined as the ratio of $\Delta\theta_{SPR}$ (with SiO$_2$ grating) to $\Delta\theta_{SPR}$ (without SiO$_2$ grating) was measured to be 2.13. While the RCWA data are not presented here, the measurement was in good agreement with the numerical SEF of 2.00 for an identical configuration. Slight SEF increment in the experiments is probably attributable to a rough surface of the fabricated SiO$_2$ gratings, which can provide more rooms for target analytes attached to the sensor substrate. The surface roughness is also responsible for spatial variances in the sensitivity results. In terms of the sensitivity limit, it is found theoretically that our SPR design may yield a

maximum sensitivity of 3.00°/RIU (RIU is refractive index unit) in an air environment.

First, such sensitivity enhancement is derived from an increased surface adhesion area. Introduction of SiO$_2$ gratings increases the amount of target molecules engaged in the SPR measurement, producing a larger SPR angle shift. Considering the geometric parameters of the SiO$_2$ grating, we found that total surface reaction area of the grating-based SPR structure is 1.5 times as large as that of a bare gold substrate. Although the reduction in grating period is another efficient way to reach a better sensitivity, an abrupt decrease in SEF at around $\Lambda = 200$ nm, which is associated with an internal radiation damping [21], makes us challenging to develop a high-resolution manufacturing process for the periodicity less than 200 nm. We are currently performing relevant fabrication works by taking advantage of nonconventional lithographic techniques.

As the second mechanism of sensitivity enhancement, the near-field distributions at the vicinity of the sensor surface were calculated to verify the enhanced plasmon field intensity by subwavelength dielectric gratings. Figure 4 displays the vertical intensity profiles at the point where maximum field of E$_X$ is found. We note that among three nonzero field components of E$_X$, H$_Y$, and E$_Z$ for TM polarization, the highest correlation between the matter-field overlap and the sensor sensitivity was obtained with the intensity of E$_X$ [22]. Hence, we provide only E$_X$ field for direct comparison with the sensitivity. In Fig. 4, the peak intensity of E$_X$ was determined to be 7.2 at the surface of a gold film for a conventional SPR structure. On the other hand, the proposed SPR substrate presented the peak intensity of 19.1 at the upper right corner of SiO$_2$ grating. Obviously, the dielectric gratings allow for a significant increase in the field intensity at the binding site, which can be used to improve the sensitivity in detecting layered biomolecular interactions [23].

It is also interesting to note in Fig. 4(b) that the field intensity grows rapidly from the gold surface and reaches a maximum on top of dielectric grating and then falls exponentially along the z-axis. Considering that SPR-based substrate typically produces the peak value at the surface of thin metal film, this contrast seems probably associated with diffraction by dielectric gratings. If a grating period is comparable to a wavelength, the dielectric grating diffracts the propagating plasmon waves and redistributes the electromagnetic field intensity spatially. On the other hand, in our previous study, when the period of a dielectric grating was substantially smaller than the wavelength, maximum field intensity was obtained at the metal surface [10].

For in-depth analysis, we numerically investigated the effect of field enhancement on the detection sensitivity by varying a grating width w at a fixed period. This is based on an assumption that the dielectric grating with a larger width

Fig. 4 FDTD results of **a** bare gold substrate and **b** SPR structure with a SiO$_2$ grating of $\Lambda = 400$ nm, $w = 200$ nm, and $d = 100$ nm. Two-dimensional FDTD images calculated at $\theta_1 = 38.36°$ and $\theta_2 = 47.34°$ are normalized by the field intensity of 10
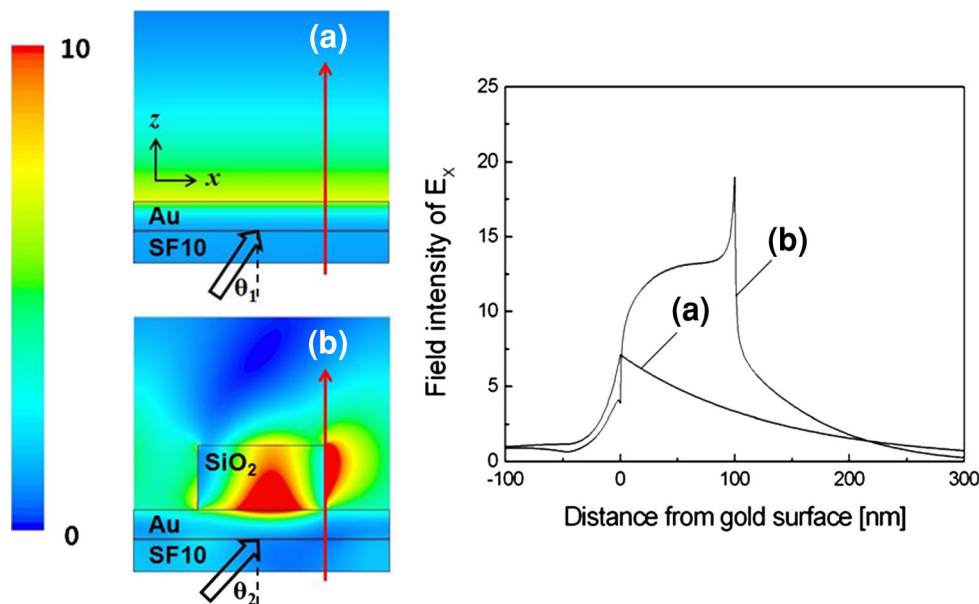
plays an important role in achieving a stronger field enhancement [24]. Dielectric grating with a larger width can provide a higher effective refractive index than the grating with a narrower width, leading to greater field intensity in the analyte region due to the presence of electromagnetic waves confined at the corrugated dielectric layer. In order to demonstrate this effectively, we considered the dielectric gratings of $\Lambda = 100$ nm, which can offer a better detection sensitivity compared to our experimental samples of $\Lambda = 400$ nm. More specifically, three cases of $w = 10$, 50 and 90 nm are chosen for proof-of-concept study, and they are obviously free from a diffraction at $\Lambda = 100$ nm.

For three different grating widths, assuming that the grating-based SPR substrates are in water ambience, which implies a practical biosensing condition, the FDTD results in Fig. 5 present near-field intensity profiles for E$_X$ component. As expected, the maximum field intensity is found at the gold surface, especially at the left corner of SiO$_2$ grating. The peak value is, respectively, obtained to be 16.0 for $w = 10$ nm, 18.9 for $w = 50$ nm, and 23.9 for $w = 90$ nm at $\Lambda = 100$ nm. This increment in the maximum intensity gives us a hint that dielectric gratings with a larger width can be more advantageous in terms of the sensitivity, although the total surface reaction area remains constant regardless of the grating width if the grating period and depth are fixed.

Next, the sensitivity of the SPR biosensor with a dielectric grating was calculated using RCWA method. The biointeraction was presumed to form a 2-nm-thick homogeneous layer onto the sensor substrate, and its refractive index n_{BL} was changed from 1.40 (i.e., ligand immobilization) to 1.50 (i.e., target attachment) in water solution.
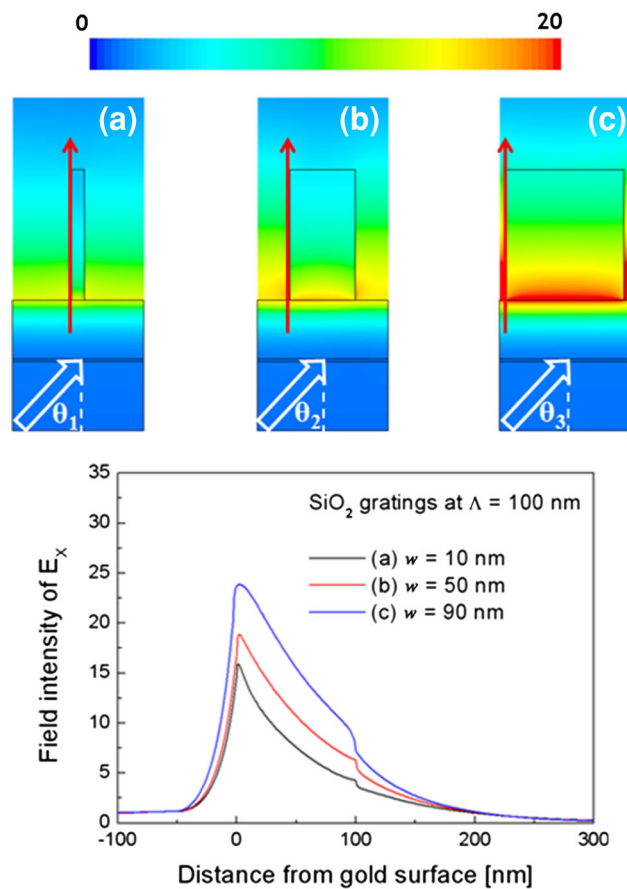

Fig. 5 FDTD results of the E$_X$ field intensity when the width of SiO$_2$ grating increases from 10 to 90 nm. The grating period and depth are fixed at $\Lambda = 100$ nm and $d = 100$ nm. In water ambience, the incidence angles are found to be **a** $\theta_1 = 60.43°$ at $w = 10$ nm, **b** $\theta_2 = 64.07°$ at $w = 50$ nm, and **c** $\theta_3 = 68.33°$ at $w = 90$ nm, respectively. The FDTD images are normalized by the field intensity of 20

We calculated the SPR angle shift due to the refractive index change of the binding layer. While SPR curves for conventional SPR system are not shown, the resonance angles are found to be 59.75° for $n_{BL} = 1.40$ and 59.94° for $n_{BL} = 1.50$; thus, the resonance shift is 0.19°, and its sensitivity is 1.9°/RIU. Also, as a quantitative metric of field-matter interaction, we define an overlap integral (OI) of field intensity as given by

$$OI = \frac{1}{\Lambda} \int_{x=0}^{x=\Lambda} \int_{z=0}^{z=\infty} \Delta n_{BL}(x,z) \cdot |E_X(x,z)|^2 dz dx, \quad (1)$$

where x and z represent the horizontal and vertical axes. Δn_{BL} is a refractive index change caused by the binding event of target molecules and therefore, in our numerical model, $\Delta n_{BL} = 0.10$ within the 2-nm-thick binding layer and otherwise, $\Delta n_{BL} = 0$.

After RCWA and FDTD computations for SiO$_2$ gratings of $\Lambda = 100$ nm, the near-field and sensor sensitivity characteristics are listed in Table 1. When a grating width increases, the OI and sensor sensitivity show a slight increment. This fairly small increase in OI and sensitivity is due to the refractive index of a dielectric material. If refractive index contrasts between a dielectric grating and an aqueous ambience is relatively small, fewer electromagnetic fields will be guided and confined at the analyte region by the corrugated dielectric grating. In this regard, we should recognize the need for applying a higher refractive index material as a dielectric grating. For example, when PMMA with a refractive index of 1.490 at $\lambda = 633$ nm [19] is substituted for SiO$_2$, the near-field distributions are illustrated in Fig. 6. The qualitative trends of increased peak intensity with a larger width resemble the results obtained by the SiO$_2$ grating. For a grating width of 90 nm, the maximum EX field intensity at the gold surface dramatically increases up to 31.2, and this substantial growth leads to the most sensitive properties as listed in Table 2. It should be also emphasized that for individual grating widths, PMMA gratings produce a better performance than SiO$_2$ gratings and the contrast in OI and sensitivity values becomes larger with an increasing width. Summarizing the results, we suggest that one can significantly improve the sensitivity of the proposed SPR biosensor by introducing a dielectric grating with a higher refractive index and a larger width, while additional optimization of geometric parameters of dielectric gratings is required for obtaining stronger field enhancement. In terms of actual implementation, fabricating the optimized SPR structures in a reproducible manner and guiding biointeractions into the extremely narrow gap still remain a challenge.

Table 1 Near-field and sensitivity characteristics of SPR substrate with SiO$_2$ gratings when the period and thickness are 100 nm

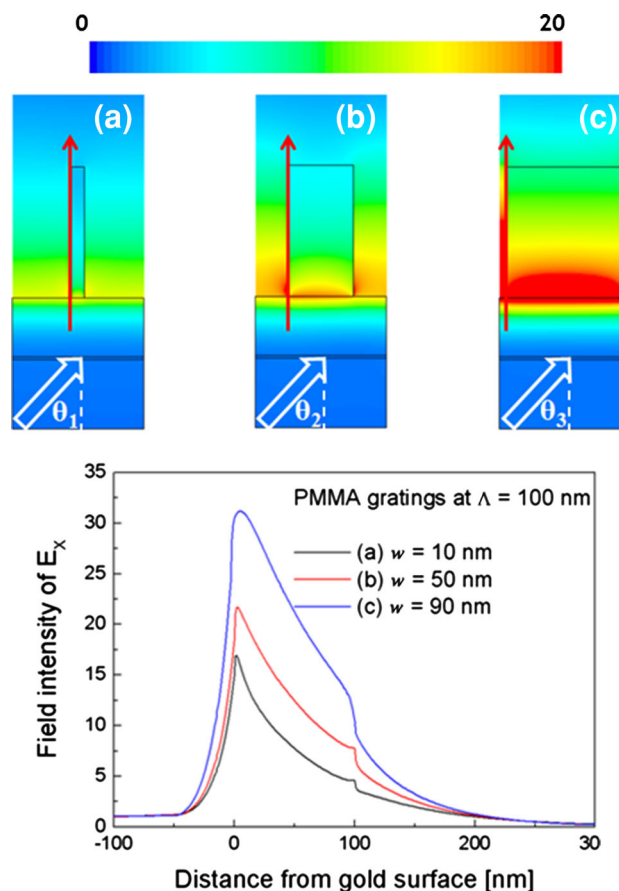| Grating width (nm)	Peak intensity of Ex	OI	Sensitivity (°/RIU)
10	16.0	8.46	4.5
50	18.9	9.42	4.6
90	23.9	11.67	4.8

Fig. 6 FDTD results of the E$_X$ field intensity when the width of PMMA grating increases from 10 to 90 nm. The grating period and depth are fixed at $\Lambda = 100$ nm and $d = 100$ nm. In water ambience, the incidence angles are found to be **a** $\theta_1 = 60.73°$ at $w = 10$ nm, **b** $\theta_2 = 65.84°$ at $w = 50$ nm, and **c** $\theta_3 = 72.35°$ at $w = 90$ nm, respectively. The FDTD images are normalized by the field intensity of 20

Table 2 Near-field and sensitivity characteristics of SPR substrate with PMMA gratings when the period and thickness are 100 nm

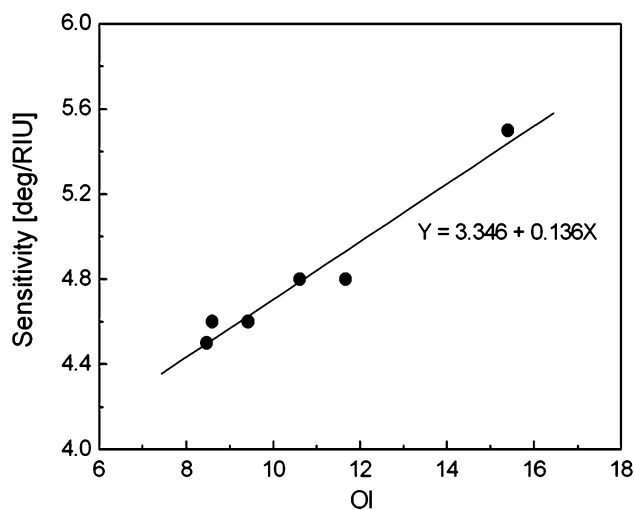| Grating width (nm)	Peak intensity of Ex	OI	Sensitivity (°/RIU)
10	17.0	8.60	4.6
50	21.7	10.62	4.8
90	31.2	15.41	5.5

Fig. 7 Correlation analysis between sensor sensitivity and OI for SiO$_2$ and PMMA gratings when the grating width is varied. The grating period and thickness are fixed at 100 nm. The solid line is the linear fit

In the final part of discussion, by combining the results in Tables 1 and 2, we briefly demonstrate the correlation between OI and sensitivity. When the two factors are directly compared in Fig. 7, it is found that the sensitivity is highly correlated with the OI. A linear relationship is evident with a correlation coefficient R = 0.9776. This strong correlation between OI and sensitivity shows an interesting possibility that the OI can be a useful tool to assess the performance of plasmonic biosensors that address enhancement of detection sensitivity.

4 Conclusion

In this study, we demonstrated an alternative yet effective approach to enhance the sensor sensitivity by incorporating subwavelength dielectric gratings on a thin gold film. A large-area pattern of 400-nm-period and 100-nm-depth SiO$_2$ gratings was successfully fabricated using nanoimprint lithography and silicon fabrication techniques. The experimental results exhibited that the dielectric grating-based SPR structure provided a sensitivity improvement by more than 2 times, compared with the case of a bare gold film. This is attributed to the increased surface reaction area and the enhanced plasmon field intensity. The measured sensitivity enhancement was in good agreement with the numerical analyses based on the RCWA. In particular, when the grating period and the thickness are fixed, the field-matter interaction tends to increase with the grating width, which is attributed to the confinement of electromagnetic fields within the corrugated dielectric waveguide layer. As a future direction, optimization of structural parameters of a dielectric grating will be necessary to produce a stronger field enhancement for high-sensitivity plasmonic sensors.

References

1. W.P. Hu, S.-J. Chen, K.-T. Huang, J.H. Hsu, W.Y. Chen, G.L. Chang, K.-A. Lai, Biosens. Bioelectron. **19**, 1465 (2004)
2. G.G. Nenninger, P. Tobiška, J. Homola, S.S. Yee, Sens. Actuators, B **74**, 145 (2001)
3. K.M. Byun, S.J. Kim, D. Kim, Opt. Express **13**, 3737 (2005)
4. L. He, M.D. Musick, S.R. Nicewarner, F.G. Salinas, S.J. Benkovic, M.J. Natan, C.D. Keating, J. Am. Chem. Soc. **122**, 9071 (2000)
5. M.-H. Chiu, S.-F. Wang, R.-S. Chang, Opt. Lett. **30**, 233 (2005)
6. A. Lahav, M. Auslender, I. Abdulhalim, Opt. Lett. **33**, 2539 (2008)
7. A. Shalabney, I. Abdulhalim, Sens. Actuators, A **159**, 24 (2010)
8. K.M. Byun, S.J. Kim, D. Kim, Appl. Opt. **46**, 5703 (2007)
9. K.M. Byun, N.-H. Kim, J.W. Leem, J.S. Yu, Appl. Phys. B **107**, 803 (2012)
10. W.K. Jung, N.-H. Kim, K.M. Byun, Appl. Opt. **51**, 4722 (2012)
11. K. Kim, D.J. Kim, S. Moon, D. Kim, K.M. Byun, Nanotechnology **20**, 315501 (2009)
12. A. Boltasseva, J. Opt. A: Pure Appl. Opt. **11**, 114001 (2009)
13. B.-J. Jeon, M.-H. Kim, J.-C. Pyun, Sens. Actuators, B **154**, 89 (2011)
14. K.M. Byun, S.J. Yoon, D. Kim, S.J. Kim, Opt. Lett. **32**, 1902 (2007)
15. L. Malic, B. Cui, T. Veres, M. Tabrizian, Opt. Lett. **32**, 3092 (2007)
16. M.G. Moharam, T.K. Gaylord, J. Opt. Soc. Am. A: **3**, 1780 (1986)
17. L. Li, J. Opt. Soc. Am. A: **10**, 2581 (1993)
18. L. Li, C.W. Haggans, J. Opt. Soc. Am. A: **10**, 1184 (1993)
19. E.D. Palik, *Handbook of Optical Constants of Solids* (Academic, Orlando, 1985)
20. M. Piliarik, J. Homola, Opt. Express **17**, 16505 (2009)
21. S.H. Choi, S.J. Kim, K.M. Byun, Appl. Opt. **48**, 2924 (2009)
22. W. Lee, D. Kim, J. Opt. Soc. Am. A: **29**, 1367 (2012)
23. K. Ma, D.J. Kim, K. Kim, S. Moon, D. Kim, IEEE J. Sel. Topics Quantum Electron. **16**, 1004 (2010)
24. J. Li, D. Fattal, Z. Li, Appl. Phys. Lett. **94**, 263114 (2009)